

Search for a Narrow Resonance in e^+e^- to Four Lepton Final States

The *BABAR* Collaboration

October 29, 2018

Abstract

Motivated by recent models proposing a hidden sector with \sim GeV scale force carriers, we present a search for a narrow dilepton resonance in 4 lepton final states using 536 fb^{-1} collected by the *BABAR* detector. We search for the reaction, $e^+e^- \rightarrow W'W' \rightarrow (l^+l^-)(l'^+l'^-)$, where the leptons carry the full 4-momentum and the two dilepton pair invariant masses are equal. We do not observe a significant signal and we set 90% upper limits of $\sigma(e^+e^- \rightarrow W'W' \rightarrow e^+e^-e^+e^-) < (15 - 70) \text{ ab}$, $\sigma(e^+e^- \rightarrow W'W' \rightarrow e^+e^-\mu^+\mu^-) < (15 - 40) \text{ ab}$, and $\sigma(e^+e^- \rightarrow W'W' \rightarrow \mu^+\mu^-\mu^+\mu^-) < (11 - 17) \text{ ab}$ in the W' mass range between 0.24 and $5.3 \text{ GeV}/c^2$. Under the assumption that the W' coupling to electrons and muons is the same, we obtain a combined upper limit of $\sigma(e^+e^- \rightarrow W'W' \rightarrow l^+l^-l'^+l'^-) < (25 - 60) \text{ ab}$. Using these limits, we constrain the product of the SM-dark sector mixing and the dark coupling constant in the case of a non-Abelian Higgsed dark sector.

Submitted to the XXIV International Symposium on Lepton Photon
Interactions at High Energies,
17 August—22 August 2009, Hamburg, Germany.

SLAC National Accelerator Laboratory, Stanford University, Stanford, CA 94309

Work supported in part by Department of Energy contract DE-AC02-76SF00515.

The BABAR Collaboration,

B. Aubert, Y. Karyotakis, J. P. Lees, V. Poireau, E. Prencipe, X. Prudent, V. Tisserand
*Laboratoire d'Annecy-le-Vieux de Physique des Particules (LAPP), Université de Savoie, CNRS/IN2P3,
F-74941 Annecy-Le-Vieux, France*

J. Garra Tico, E. Grauges
Universitat de Barcelona, Facultat de Fisica, Departament ECM, E-08028 Barcelona, Spain

M. Martinelli^{ab}, A. Palano^{ab}, M. Pappagallo^{ab}
INFN Sezione di Bari^a; Dipartimento di Fisica, Università di Bari^b, I-70126 Bari, Italy

G. Eigen, B. Stugu, L. Sun
University of Bergen, Institute of Physics, N-5007 Bergen, Norway

M. Battaglia, D. N. Brown, B. Hooberman, L. T. Kerth, Yu. G. Kolomensky, G. Lynch, I. L. Osipenkov,
K. Tackmann, T. Tanabe
Lawrence Berkeley National Laboratory and University of California, Berkeley, California 94720, USA

C. M. Hawkes, N. Soni, A. T. Watson
University of Birmingham, Birmingham, B15 2TT, United Kingdom

H. Koch, T. Schroeder
Ruhr Universität Bochum, Institut für Experimentalphysik 1, D-44780 Bochum, Germany

D. J. Asgeirsson, C. Hearty, T. S. Mattison, J. A. McKenna
University of British Columbia, Vancouver, British Columbia, Canada V6T 1Z1

M. Barrett, A. Khan, A. Randle-Conde
Brunel University, Uxbridge, Middlesex UB8 3PH, United Kingdom

V. E. Blinov, A. D. Bukin,¹ A. R. Buzykaev, V. P. Druzhinin, V. B. Golubev, A. P. Onuchin,
S. I. Serednyakov, Yu. I. Skovpen, E. P. Solodov, K. Yu. Todyshev
Budker Institute of Nuclear Physics, Novosibirsk 630090, Russia

M. Bondioli, S. Curry, I. Eschrich, D. Kirkby, A. J. Lankford, P. Lund, M. Mandelkern, E. C. Martin,
D. P. Stoker
University of California at Irvine, Irvine, California 92697, USA

H. Atmacan, J. W. Gary, F. Liu, O. Long, G. M. Vitug, Z. Yasin
University of California at Riverside, Riverside, California 92521, USA

V. Sharma
University of California at San Diego, La Jolla, California 92093, USA

C. Campagnari, T. M. Hong, D. Kovalskyy, M. A. Mazur, J. D. Richman
University of California at Santa Barbara, Santa Barbara, California 93106, USA

¹Deceased

T. W. Beck, A. M. Eisner, C. A. Heusch, J. Kroseberg, W. S. Lockman, A. J. Martinez, T. Schalk,
B. A. Schumm, A. Seiden, L. Wang, L. O. Winstrom
University of California at Santa Cruz, Institute for Particle Physics, Santa Cruz, California 95064, USA

C. H. Cheng, D. A. Doll, B. Echenard, F. Fang, D. G. Hitlin, I. Narsky, P. Ongmongkolkul, T. Piatenko,
F. C. Porter
California Institute of Technology, Pasadena, California 91125, USA

R. Andreassen, G. Mancinelli, B. T. Meadows, K. Mishra, M. D. Sokoloff
University of Cincinnati, Cincinnati, Ohio 45221, USA

P. C. Bloom, W. T. Ford, A. Gaz, J. F. Hirschauer, M. Nagel, U. Nauenberg, J. G. Smith, S. R. Wagner
University of Colorado, Boulder, Colorado 80309, USA

R. Ayad,² W. H. Toki
Colorado State University, Fort Collins, Colorado 80523, USA

E. Feltresi, A. Hauke, H. Jasper, T. M. Karbach, J. Merkel, A. Petzold, B. Spaan, K. Wacker
Technische Universität Dortmund, Fakultät Physik, D-44221 Dortmund, Germany

M. J. Kobel, R. Nogowski, K. R. Schubert, R. Schwierz
Technische Universität Dresden, Institut für Kern- und Teilchenphysik, D-01062 Dresden, Germany

D. Bernard, E. Latour, M. Verderi
Laboratoire Leprince-Ringuet, CNRS/IN2P3, Ecole Polytechnique, F-91128 Palaiseau, France

P. J. Clark, S. Playfer, J. E. Watson
University of Edinburgh, Edinburgh EH9 3JZ, United Kingdom

M. Andreotti^{ab}, D. Bettoni^a, C. Bozzi^a, R. Calabrese^{ab}, A. Cecchi^{ab}, G. Cibinetto^{ab}, E. Fioravanti^{ab}
P. Franchini^{ab}, E. Luppi^{ab}, M. Menerato^{ab}, M. Negrini^{ab}, A. Petrella^{ab}, L. Piemontese^a, V. Santoro^{ab}
INFN Sezione di Ferrara^a; Dipartimento di Fisica, Università di Ferrara^b, I-44100 Ferrara, Italy

R. Baldini-Ferrolli, A. Calcaterra, R. de Sangro, G. Finocchiaro, S. Pacetti, P. Patteri, I. M. Peruzzi,³
M. Piccolo, M. Rama, A. Zallo
INFN Laboratori Nazionali di Frascati, I-00044 Frascati, Italy

R. Contri^{ab}, E. Guido^{ab}, M. Lo Vetere^{ab}, M. R. Monge^{ab}, S. Passaggio^a, C. Patrignani^{ab}, E. Robutti^a,
S. Tosi^{ab}
INFN Sezione di Genova^a; Dipartimento di Fisica, Università di Genova^b, I-16146 Genova, Italy

M. Morii
Harvard University, Cambridge, Massachusetts 02138, USA

A. Adametz, J. Marks, S. Schenk, U. Uwer
Universität Heidelberg, Physikalisches Institut, Philosophenweg 12, D-69120 Heidelberg, Germany

²Now at Temple University, Philadelphia, Pennsylvania 19122, USA

³Also with Università di Perugia, Dipartimento di Fisica, Perugia, Italy

F. U. Bernlochner, H. M. Lacker, T. Lueck, A. Volk
Humboldt-Universität zu Berlin, Institut für Physik, Newtonstr. 15, D-12489 Berlin, Germany

P. D. Dauncey, M. Tibbetts
Imperial College London, London, SW7 2AZ, United Kingdom

P. K. Behera, M. J. Charles, U. Mallik
University of Iowa, Iowa City, Iowa 52242, USA

J. Cochran, H. B. Crawley, L. Dong, V. Eyges, W. T. Meyer, S. Prell, E. I. Rosenberg, A. E. Rubin
Iowa State University, Ames, Iowa 50011-3160, USA

Y. Y. Gao, A. V. Gritsan, Z. J. Guo
Johns Hopkins University, Baltimore, Maryland 21218, USA

N. Arnaud, A. D’Orazio, M. Davier, D. Derkach, J. Firmino da Costa, G. Grosdidier, F. Le Diberder, V. Lepeltier, A. M. Lutz, B. Malaescu, P. Roudeau, M. H. Schune, J. Serrano, V. Sordini,⁴ A. Stocchi, G. Wormser

Laboratoire de l’Accélérateur Linéaire, IN2P3/CNRS et Université Paris-Sud 11, Centre Scientifique d’Orsay, B. P. 34, F-91898 Orsay Cedex, France

D. J. Lange, D. M. Wright
Lawrence Livermore National Laboratory, Livermore, California 94550, USA

I. Bingham, J. P. Burke, C. A. Chavez, J. R. Fry, E. Gabathuler, R. Gamet, D. E. Hutchcroft, D. J. Payne, C. Touramanis

University of Liverpool, Liverpool L69 7ZE, United Kingdom

A. J. Bevan, C. K. Clarke, F. Di Lodovico, R. Sacco, M. Sigamani
Queen Mary, University of London, London, E1 4NS, United Kingdom

G. Cowan, S. Paramesvaran, A. C. Wren
University of London, Royal Holloway and Bedford New College, Egham, Surrey TW20 0EX, United Kingdom

D. N. Brown, C. L. Davis
University of Louisville, Louisville, Kentucky 40292, USA

A. G. Denig, M. Fritsch, W. Gradl, A. Hafner
Johannes Gutenberg-Universität Mainz, Institut für Kernphysik, D-55099 Mainz, Germany

K. E. Alwyn, D. Bailey, R. J. Barlow, G. Jackson, G. D. Lafferty, T. J. West, J. I. Yi
University of Manchester, Manchester M13 9PL, United Kingdom

J. Anderson, C. Chen, A. Jawahery, D. A. Roberts, G. Simi, J. M. Tuggle
University of Maryland, College Park, Maryland 20742, USA

C. Dallapiccola, E. Salvati
University of Massachusetts, Amherst, Massachusetts 01003, USA

⁴Also with Università di Roma La Sapienza, I-00185 Roma, Italy

R. Cowan, D. Dujmic, P. H. Fisher, S. W. Henderson, G. Sciolla, M. Spitznagel, R. K. Yamamoto, M. Zhao
Massachusetts Institute of Technology, Laboratory for Nuclear Science, Cambridge, Massachusetts 02139, USA

P. M. Patel, S. H. Robertson, M. Schram
McGill University, Montréal, Québec, Canada H3A 2T8

P. Biassoni^{ab}, A. Lazzaro^{ab}, V. Lombardo^a, F. Palombo^{ab}, S. Stracka^{ab}
INFN Sezione di Milano^a; Dipartimento di Fisica, Università di Milano^b, I-20133 Milano, Italy

L. Cremaldi, R. Godang,⁵ R. Kroeger, P. Sonnek, D. J. Summers, H. W. Zhao
University of Mississippi, University, Mississippi 38677, USA

X. Nguyen, M. Simard, P. Taras
Université de Montréal, Physique des Particules, Montréal, Québec, Canada H3C 3J7

H. Nicholson
Mount Holyoke College, South Hadley, Massachusetts 01075, USA

G. De Nardo^{ab}, L. Lista^a, D. Monorchio^{ab}, G. Onorato^{ab}, C. Sciacca^{ab}
INFN Sezione di Napoli^a; Dipartimento di Scienze Fisiche, Università di Napoli Federico II^b, I-80126 Napoli, Italy

G. Raven, H. L. Snoek
NIKHEF, National Institute for Nuclear Physics and High Energy Physics, NL-1009 DB Amsterdam, The Netherlands

C. P. Jessop, K. J. Knoepfel, J. M. LoSecco, W. F. Wang
University of Notre Dame, Notre Dame, Indiana 46556, USA

L. A. Corwin, K. Honscheid, H. Kagan, R. Kass, J. P. Morris, A. M. Rahimi, S. J. Sekula
Ohio State University, Columbus, Ohio 43210, USA

N. L. Blount, J. Brau, R. Frey, O. Igonkina, J. A. Kolb, M. Lu, R. Rahmat, N. B. Sinev, D. Strom,
J. Strube, E. Torrence
University of Oregon, Eugene, Oregon 97403, USA

G. Castelli^{ab}, N. Gagliardi^{ab}, M. Margoni^{ab}, M. Morandin^a, M. Posocco^a, M. Rotondo^a, F. Simonetto^{ab},
R. Stroili^{ab}, C. Voci^{ab}
INFN Sezione di Padova^a; Dipartimento di Fisica, Università di Padova^b, I-35131 Padova, Italy

P. del Amo Sanchez, E. Ben-Haim, G. R. Bonneaud, H. Briand, J. Chauveau, O. Hamon, Ph. Leruste,
G. Marchiori, J. Ocariz, A. Perez, J. Prendki, S. Sitt
Laboratoire de Physique Nucléaire et de Hautes Energies, IN2P3/CNRS, Université Pierre et Marie Curie-Paris6, Université Denis Diderot-Paris7, F-75252 Paris, France

L. Gladney
University of Pennsylvania, Philadelphia, Pennsylvania 19104, USA

⁵Now at University of South Alabama, Mobile, Alabama 36688, USA

M. Biasini^{ab}, E. Manoni^{ab}

INFN Sezione di Perugia^a; Dipartimento di Fisica, Università di Perugia^b, I-06100 Perugia, Italy

C. Angelini^{ab}, G. Batignani^{ab}, S. Bettarini^{ab}, G. Calderini^{ab},⁶ M. Carpinelli^{ab},⁷ A. Cervelli^{ab}, F. Forti^{ab},
M. A. Giorgi^{ab}, A. Lusiani^{ac}, M. Morganti^{ab}, N. Neri^{ab}, E. Paoloni^{ab}, G. Rizzo^{ab}, J. J. Walsh^a

*INFN Sezione di Pisa^a; Dipartimento di Fisica, Università di Pisa^b; Scuola Normale Superiore di Pisa^c,
I-56127 Pisa, Italy*

D. Lopes Pegna, C. Lu, J. Olsen, A. J. S. Smith, A. V. Telnov

Princeton University, Princeton, New Jersey 08544, USA

F. Anulli^a, E. Baracchini^{ab}, G. Cavoto^a, R. Faccini^{ab}, F. Ferrarotto^a, F. Ferroni^{ab}, M. Gaspero^{ab},
P. D. Jackson^a, L. Li Gioi^a, M. A. Mazzone^a, S. Morganti^a, G. Piredda^a, F. Renga^{ab}, C. Voena^a

INFN Sezione di Roma^a; Dipartimento di Fisica, Università di Roma La Sapienza^b, I-00185 Roma, Italy

M. Ebert, T. Hartmann, H. Schröder, R. Waldi

Universität Rostock, D-18051 Rostock, Germany

T. Adye, B. Franek, E. O. Olaiya, F. F. Wilson

Rutherford Appleton Laboratory, Chilton, Didcot, Oxon, OX11 0QX, United Kingdom

S. Emery, L. Esteve, G. Hamel de Monchenault, W. Kozanecki, G. Vasseur, Ch. Yèche, M. Zito

CEA, Irfu, SPP, Centre de Saclay, F-91191 Gif-sur-Yvette, France

M. T. Allen, D. Aston, D. J. Bard, R. Bartoldus, J. F. Benitez, R. Cenci, J. P. Coleman, M. R. Convery,
J. C. Dingfelder, J. Dorfan, G. P. Dubois-Felsmann, W. Dunwoodie, R. C. Field, M. Franco Sevilla,
B. G. Fulsom, A. M. Gabareen, M. T. Graham, P. Grenier, C. Hast, W. R. Innes, J. Kaminski,
M. H. Kelsey, H. Kim, P. Kim, M. L. Kocian, D. W. G. S. Leith, S. Li, B. Lindquist, S. Luitz, V. Luth,
H. L. Lynch, D. B. MacFarlane, H. Marsiske, R. Messner,⁸ D. R. Muller, H. Neal, S. Nelson,
C. P. O'Grady, I. Ofte, M. Perl, B. N. Ratcliff, A. Roodman, A. A. Salnikov, R. H. Schindler,
J. Schwiening, A. Snyder, D. Su, M. K. Sullivan, K. Suzuki, S. K. Swain, J. M. Thompson, J. Va'vra,
A. P. Wagner, M. Weaver, C. A. West, W. J. Wisniewski, M. Wittgen, D. H. Wright, H. W. Wulsin,
A. K. Yarritu, C. C. Young, V. Ziegler

SLAC National Accelerator Laboratory, Stanford, California 94309 USA

X. R. Chen, H. Liu, W. Park, M. V. Purohit, R. M. White, J. R. Wilson

University of South Carolina, Columbia, South Carolina 29208, USA

M. Bellis, P. R. Burchat, A. J. Edwards, T. S. Miyashita

Stanford University, Stanford, California 94305-4060, USA

S. Ahmed, M. S. Alam, J. A. Ernst, B. Pan, M. A. Saeed, S. B. Zain

State University of New York, Albany, New York 12222, USA

A. Soffer

Tel Aviv University, School of Physics and Astronomy, Tel Aviv, 69978, Israel

⁶Also with Laboratoire de Physique Nucléaire et de Hautes Energies, IN2P3/CNRS, Université Pierre et Marie Curie-Paris6, Université Denis Diderot-Paris7, F-75252 Paris, France

⁷Also with Università di Sassari, Sassari, Italy

⁸Deceased

S. M. Spanier, B. J. Wogslund

University of Tennessee, Knoxville, Tennessee 37996, USA

R. Eckmann, J. L. Ritchie, A. M. Ruland, C. J. Schilling, R. F. Schwitters, B. C. Wray

University of Texas at Austin, Austin, Texas 78712, USA

B. W. Drummond, J. M. Izen, X. C. Lou

University of Texas at Dallas, Richardson, Texas 75083, USA

F. Bianchi^{ab}, D. Gamba^{ab}, M. Pelliccioni^{ab}

INFN Sezione di Torino^a; Dipartimento di Fisica Sperimentale, Università di Torino^b, I-10125 Torino, Italy

M. Bomben^{ab}, L. Bosisio^{ab}, C. Cartaro^{ab}, G. Della Ricca^{ab}, L. Lanceri^{ab}, L. Vitale^{ab}

INFN Sezione di Trieste^a; Dipartimento di Fisica, Università di Trieste^b, I-34127 Trieste, Italy

V. Azzolini, N. Lopez-March, F. Martinez-Vidal, D. A. Milanes, A. Oyanguren

IFIC, Universitat de Valencia-CSIC, E-46071 Valencia, Spain

J. Albert, Sw. Banerjee, B. Bhuyan, H. H. F. Choi, K. Hamano, G. J. King, R. Kowalewski,
M. J. Lewczuk, I. M. Nugent, J. M. Roney, R. J. Sobie

University of Victoria, Victoria, British Columbia, Canada V8W 3P6

T. J. Gershon, P. F. Harrison, J. Ilic, T. E. Latham, G. B. Mohanty, E. M. T. Puccio

Department of Physics, University of Warwick, Coventry CV4 7AL, United Kingdom

H. R. Band, X. Chen, S. Dasu, K. T. Flood, Y. Pan, R. Prepost, C. O. Vuosalo, S. L. Wu

University of Wisconsin, Madison, Wisconsin 53706, USA

1 Introduction

Recent cosmic ray measurements of the electron and positron flux from ATIC[1], FERMI[2], and PAMELA[3] have spectra which are not well described by galactic cosmic ray models such as GALPROP[4]. For instance, PAMELA shows an increase in the positron/electron fraction with increasing energy. No corresponding increase in the antiproton spectrum is observed. There have been two main approaches attempting to explain these features: astrophysical sources (particularly from undetected, nearby pulsars)[5] and annihilating or decaying dark matter.

Arkani-Hamed *et al.*[6] have introduced a class of theories containing a new “dark force” and a light, hidden sector. In this model, the ATIC and PAMELA signals are due to dark matter particles with mass $\sim 400 - 800 \text{ GeV}/c^2$ annihilating into the gauge boson force carrier with mass $\sim 1 \text{ GeV}/c^2$, which they dub the ϕ , which subsequently decays to Standard Model particles. If the ϕ mass is below twice the proton mass, decays to $p\bar{p}$ are kinematically forbidden allowing only decays to states like e^+e^- , $\mu^+\mu^-$, and $\pi\pi$. If the dark force is non-Abelian, this theory can also accommodate the 511 keV signal found by the INTEGRAL satellite [7] and the DAMA modulation data [8].

The dark sector couples to the Standard Model through kinetic mixing with the photon. Thus low-energy/high luminosity e^+e^- experiments like *BABAR* are in excellent position to probe these theories. Recent papers by Batell *et al.* [9] and Essig *et al.* [10] have discussed the prospects for finding evidence for the dark sector at the B-Factories in the Abelian and non-Abelian cases, respectively. In the Abelian case, the signatures would be $e^+e^- \rightarrow \gamma\phi \rightarrow \gamma l^+l^-$ or $e^+e^- \rightarrow \phi h' \rightarrow 3(l^+l^-)$ (where h' is a “dark Higgs”). There are actually two non-Abelian scenarios: the Higgsed case and the confined case (“dark QCD”). In the Higgsed case there are at least three dark particles in play: A' which mixes with the photon, another gauge boson W' , and the dark Higgs h' . In this regime, signatures are $e^+e^- \rightarrow W'W' \rightarrow l^+l^-l^+l^-$ (via a virtual A') and $e^+e^- \rightarrow \gamma A'(\rightarrow W'W') \rightarrow \gamma l^+l^-l^+l^-$, plus “Higgs'-strahlung” processes which may lead to missing energy. Finally, the confined case could lead to a proliferation of “dark mesons”, whose lowest mass states decay to leptons. Depending on the scenario and the coupling between the Standard Model and dark sectors, cross sections could be as large as a few femtobarns at *BABAR* which would translate to hundreds of events observed in the detector.

In this note we describe a search for the W' in the reaction $e^+e^- \rightarrow W'W' \rightarrow l^+l^-l^+l^-$ in exclusive 4-lepton final states, where we require that the four leptons carry the full center of mass energy and that the two dilepton pairs have the same invariant mass.

2 The *BABAR* Detector and Dataset

The data used in this analysis were collected with the *BABAR* detector at the PEP-II asymmetric energy e^+e^- storage rings between 1999 and 2008 and correspond to an integrated luminosity of 536 fb^{-1} . This data was mostly at the $\Upsilon(4S)$ peak but it also includes collisions at the $\Upsilon(2S)$ and $\Upsilon(3S)$ as well as off-resonant data.

To study signal efficiency and resolution, $e^+e^- \rightarrow W'W' \rightarrow l^+l^-l^+l^-$ Monte Carlo (MC) samples were generated (where $l=e$ or μ) for different values of W' mass using the MadGraph event generator[11]. There were 10^4 events generated at each mass value of: 0.3, 0.4, 0.5, 0.7, 1.0, 1.5, 2.0, 3.0, 4.0, and 5.0 $\text{ GeV}/c^2$. To study backgrounds, we have inspected $B\bar{B}$ ($\sim 3x$ luminosity), uds , $c\bar{c}$, and $\tau\tau$ MC samples (each $\sim 1x$ luminosity). In addition we created 4-lepton QED samples using the diag36 event generator[12].

A detailed description of the *BABAR* detector is given in [13]. Charged-particle trajectories are measured by a five-layer, double-sided silicon vertex tracker (SVT) and a 40-layer drift chamber (DCH) coaxial with a 1.5 T magnetic field. Charged-particle identification is achieved by combining the information from a ring-imaging Cherenkov device (DIRC) with the ionization energy loss (dE/dx) measurements from the DCH and SVT. Photons are detected in a CsI(Tl) electromagnetic calorimeter (EMC) inside the coil. Muon candidates are identified in the instrumented flux return (IFR) of the superconducting solenoid. We use GEANT4-based [14] software to simulate the detector response and account for the varying beam and environmental conditions.

3 Event Selection

We search for the exclusive pair production of a narrow resonance, consistent with the detector resolution, decaying to leptons and with a mass in the range between $240 \text{ MeV}/c^2$ to $\sqrt{s}/2$. The signature is 4 leptons with zero total charge carrying the full beam momentum where the two dilepton invariant masses are equal. This topology, particularly the equal invariant masses, is quite unique and the only backgrounds are from 4-lepton QED processes. The full selection criteria are described below. We used 10% of the data as a test (*blind*) sample to choose our selection and signal extraction procedures before looking at the full dataset.

We begin by selecting events with:

- 4 charged tracks
- two leptons with $p_{\text{CM}} > 1.5 \text{ GeV}/c$
- sum of the absolute value of momentum of all tracks $> 6 \text{ GeV}/c^2$ or the total visible energy (lab) $> 8 \text{ GeV}/c^2$

We reconstruct 4-lepton candidates from combinations of two $W' \rightarrow l^+l^-$ candidates. The lepton candidates are chosen by their signatures in the EMC and IFR. The W' candidates are formed from e^+e^- or $\mu^+\mu^-$ pairs. We then select events which satisfy the following criteria:

- $[N_e, N_\mu] = [4, 0], [2, 2], \text{ or } [0, 4]$
- $M_{4\text{lepton}} > 10 \text{ GeV}/c^2$
- the helicity angle of a lepton pair, defined as the angle between the positive lepton and the lepton-pair flight direction, is required to be $|\cos(\theta_H)| < 0.95$ for each pair
- to reduce background from photon conversions, we require the flight significance, defined as the W' candidates decay length from the interaction point divided by the error, is $< 4\sigma$ for each pair
- to reduce background from radiative Bhabha events, we require the angle between the decay planes of the lepton pairs, $\phi_{DPN} > 0.2$

The 4-lepton candidate is then fit constraining the four-momentum to the total beam momentum and the vertex to the interaction point.

At this point, we can exploit the fact that both dilepton pairs for our signal events have the same invariant mass. The 2-dimensional distributions of dilepton masses for each final state after

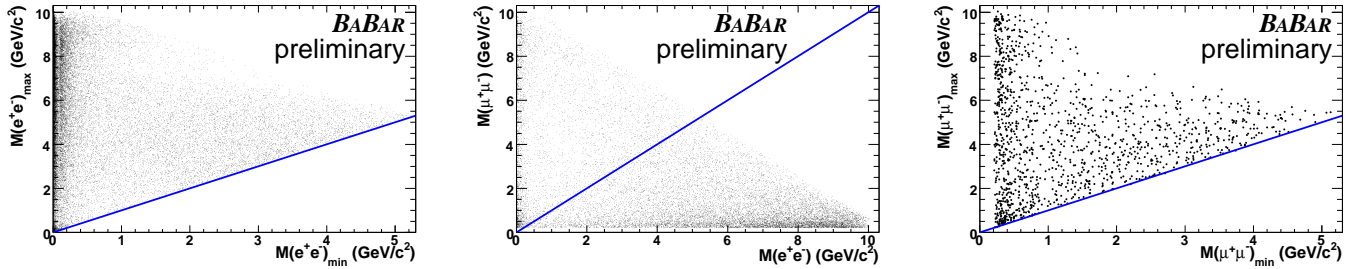


Figure 1: The dilepton invariant mass distributions from data for (left to right) $e^+e^-e^+e^-$, $e^+e^-\mu^+\mu^-$, and $\mu^+\mu^-\mu^+\mu^-$ after all other cuts. The solid lines denotes $m_1 = m_2$.

all of the above cuts for the blinding sample is shown in Figure 1. We define the transformed masses:

$$\bar{m} = (m_1 + m_2) / 2 \quad (1)$$

$$\Delta m = |m_1 - m_2| \quad (2)$$

where m_1 and m_2 are the dilepton invariant masses. The distribution of events for these variables is shown in Figure 2. We impose a cut on Δm (shown as the solid line in Figure 2) of $\Delta m < 0.25 \text{ GeV}/c^2$ for $\bar{m} < 1.0 \text{ GeV}/c^2$ and $\Delta m < 0.50 \text{ GeV}/c^2$ for $\bar{m} > 1.0 \text{ GeV}/c^2$. Because of the threshold effects in $\mu^+\mu^-\mu^+\mu^-$, we tighten the Δm cut in a linear fashion below $\bar{m} < 4 \times M(\mu)$.

In the case of the $e^+e^-e^+e^-$ and $\mu^+\mu^-\mu^+\mu^-$ final state, there are two possible l^+l^- pair combinations. If both pairings pass all cuts, the pair with the smallest value of Δm is used. For data, we see two pairings passing all cuts except the Δm cut for 25% of $e^+e^-e^+e^-$ events and for 44% of the $\mu^+\mu^-\mu^+\mu^-$ events. Table 1 shows the progressive and total efficiencies for the three different final states of $W'W' \rightarrow l^+l^-l^+l^-$ (assuming the mass of the W' is $1 \text{ GeV}/c^2$) as well as the progressive efficiency for the data. As shown in the table, the loose cut on Δm is extremely powerful at reducing the background while not affecting the signal efficiency. After all selection, there are 28303 events remaining in our data sample; of these 16531 are $e^+e^-e^+e^-$ events, 9592 are $e^+e^-\mu^+\mu^-$ events, and 2180 are $\mu^+\mu^-\mu^+\mu^-$ events.

4 Signal Extraction

Our aim is to perform a search for a narrow peak in the \bar{m} range from $240 \text{ MeV}/c^2$ up to $\sqrt{s}/2$. After the selection described in the previous section, the expected backgrounds are quite low and we have decided to perform a cut-and-count analysis in bins of \bar{m} , using the the Δm variable to define the signal and background regions. The number of observed signal events in a \bar{m} bin is then:

$$N_{sig} = N_{signal\ region} - N_{bkg\ region} \times \frac{A_{signal}}{A_{background}} \quad (3)$$

where A_{signal} ($A_{background}$) is the area of the signal (background) Δm region.

In this section, we will discuss the signal efficiency, Δm shapes (including the definition of signal and background regions) and background rates as a function of \bar{m} and the method we plan to use in extracting the signal yields and setting limits.

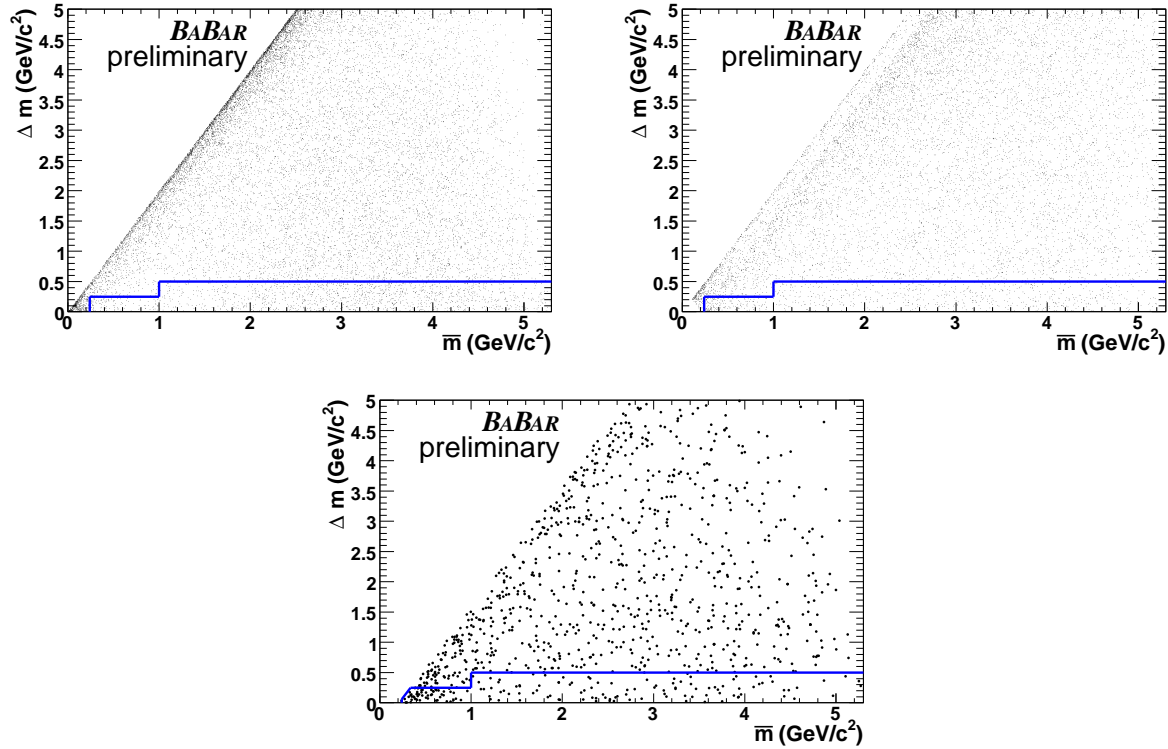


Figure 2: The transformed mass distributions, Δm vs \bar{m} , from data for (left to right) $e^+e^-e^+e^-$, $e^+e^-\mu^+\mu^-$, and $\mu^+\mu^-\mu^+\mu^-$ after all other cuts. The solid lines denotes the Δm cut value.

4.1 Efficiency and Δm resolution dependence on the W' mass

The efficiency for different generated values of the W' mass is shown in Figure 3. The efficiency decreases from $\sim 45\%$ at 1 GeV to 25 – 30% at high masses depending on the decay mode. There is a dip in efficiency for mass pairs around $500 \text{ MeV}/c^2$ which is due to the opening angle of the lepton pair at this mass coinciding with the bending angle at the EMC, precluding us from identifying the two particles for a fraction of the events. The Δm resolution also varies significantly as a function of W' mass. Figure 4 shows the distributions of Δm for four different mass values. The resolution of Δm increases with increasing W' mass. Since the background Δm distribution is basically flat and roughly constant in \bar{m} (see Section 4.2), the effect is to reduce the sensitivity at higher masses.

Figure 5 shows the values of the Δm cut which retains 90% of the signal as a function of \bar{m} . We use this cut value to define the signal ($\Delta m < cutVal$) and background ($dm > cutVal$) regions for the cut-and-count signal extraction. Recall that the maximum value of Δm is $0.25(0.5) \text{ GeV}/c^2$ for $\bar{m} < (>)1.0 \text{ GeV}/c^2$. The solid line is the result of a 4th-order polynomial fit which we use to extrapolate between \bar{m} points.

4.2 Background composition

While we ultimately use the Δm sidebands to determine our background level, we have also used MC to study the composition of the background. In generic $q\bar{q}$, $B^0\bar{B}^0$, B^+B^- , and $\tau^+\tau^-$ samples we find only a single event passing the cuts (a $q\bar{q}$ event in the 4-electron final state). From this we

Table 1: Selection efficiencies relative to the previous cut with binomial errors for the three signal decay modes assuming $M(W') = 1 \text{ GeV}/c^2$ and for onpeak data.

Cuts	Relative Efficiencies (%)			
	$\varepsilon_{W'W' \rightarrow 4e}$	$\varepsilon_{W'W' \rightarrow 2e2\mu}$	$\varepsilon_{W'W' \rightarrow 4\mu}$	ε_{data}
Preselection	61.4 ± 0.5	68.2 ± 0.5	73.4 ± 0.4	— — — —
N(tracks)=4	93.3 ± 0.3	95.5 ± 0.3	97.1 ± 0.2	83.7 ± 0.0
N(leptons)	99.9 ± 0.1	100.0 ± 0.0	100.0 ± 0.0	98.7 ± 0.0
$M(4l) > 10 \text{ GeV}$	87.2 ± 0.5	93.2 ± 0.3	98.1 ± 0.2	66.2 ± 0.0
$ \cos(\theta_H) < 0.95$	99.9 ± 0.1	99.6 ± 0.1	98.8 ± 0.1	18.2 ± 0.0
fit. sig. $< 4\sigma$	97.2 ± 0.2	96.5 ± 0.4	99.1 ± 0.1	54.6 ± 0.1
μ PID	100.0 ± 0.0	81.9 ± 0.6	70.3 ± 0.6	74.2 ± 0.1
$\phi_{DPN} > 0.2$	92.4 ± 0.4	93.2 ± 0.4	93.6 ± 0.4	37.0 ± 0.1
$\Delta(m)$	98.3 ± 0.2	99.8 ± 0.1	99.6 ± 0.1	3.8 ± 0.1
Total Efficiency	43.7 ± 0.5	44.5 ± 0.5	44.8 ± 0.5	— — — —

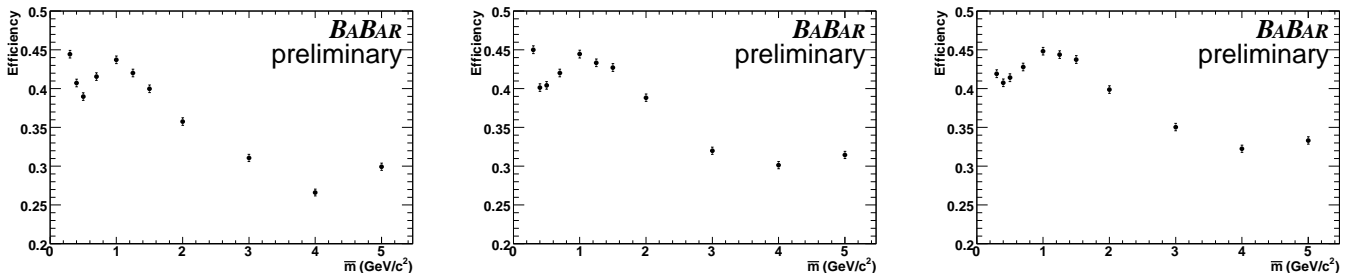


Figure 3: The signal efficiency versus W' mass for (left to right) $W'W' \rightarrow e^+e^-e^+e^-$, $W'W' \rightarrow e^+e^-\mu^+\mu^-$, and $W'W' \rightarrow \mu^+\mu^-\mu^+\mu^-$ after all cuts.

conclude that our background is dominated by QED processes.

We have generated $e^+e^-\mu^+\mu^-$ and $\mu^+\mu^-\mu^+\mu^-$ samples⁹ using the `diag36` generator and compared the MC to our selected dataset. We find good agreement both in the scale and shape between data and the four-lepton QED MC. From the MC, we expect to observe 16241 ± 250 $\mu^+\mu^-\mu^+\mu^-$ events in the full dataset while we observe 15666 ± 125 (statistical errors only). For $e^+e^-\mu^+\mu^-$ we expect 219927 ± 3450 and observe 185499 ± 431 events.

The background distributions in Δm and \overline{m} , after all selection, are shown in Figure 6. The background Δm distributions were fit with a line in different slices of \overline{m} , the slopes of which are plotted for the three modes in Figure 7, and the slopes are consistent with 0. When extracting the signal yields, we assume a uniform background distribution, and take into account the uncertainties in the slope as a systematic error. We use the full dataset for the above plots; any signal present would be completely washed out when projected onto the Δm or \overline{m} axis.

⁹Due to the enormous $e^+e^-e^+e^-$ QED cross-section, this mode is difficult to generate efficiently.

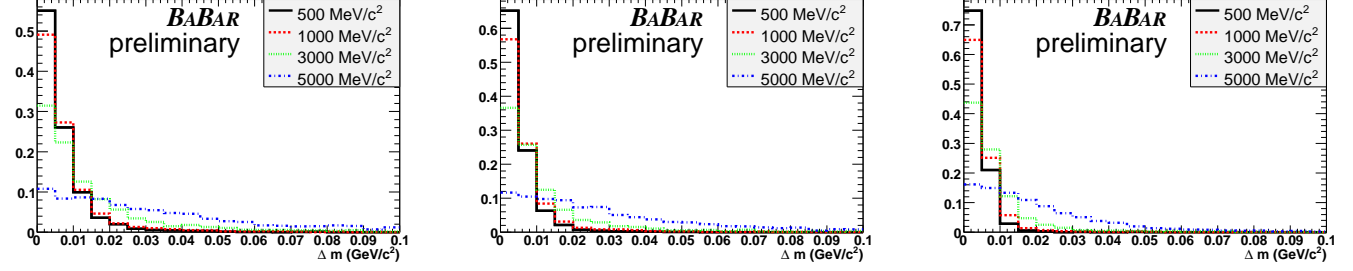


Figure 4: The Δm distributions for four different W' mass values (left to right) $W'W' \rightarrow e^+e^-e^+e^-$, $W'W' \rightarrow e^+e^-\mu^+\mu^-$, and $W'W' \rightarrow \mu^+\mu^-\mu^+\mu^-$ after all cuts.

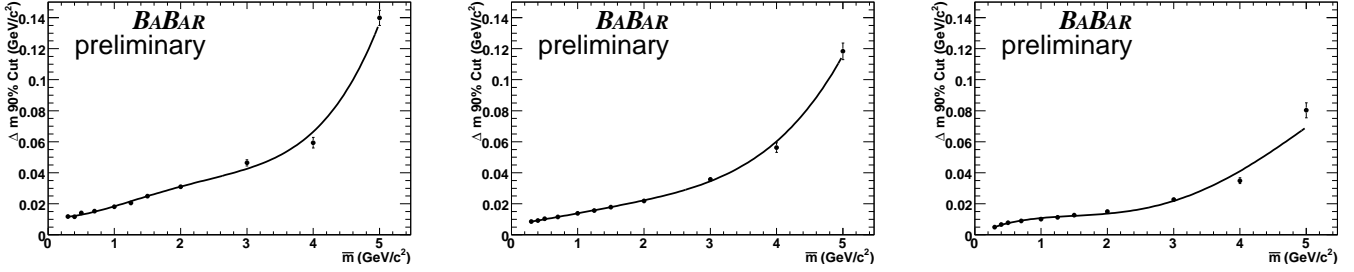


Figure 5: The values of the cut on Δm keeping 90% of signal events as a function of W' mass for (left to right) $W'W' \rightarrow e^+e^-e^+e^-$, $W'W' \rightarrow e^+e^-\mu^+\mu^-$, and $W'W' \rightarrow \mu^+\mu^-\mu^+\mu^-$. The line is a fit to a fourth order polynomial. This cut defines our signal and background region.

4.3 Signal extraction and limit setting

In this analysis, our aim is to obtain a limit (or observe a signal) for $e^+e^- \rightarrow W'W'$ as function of the presumed W' mass. To this end, search for a signal in steps of the average dilepton mass \bar{m} . We have chosen the \bar{m} bin size to be $20 \text{ MeV}/c^2$, which is a large enough range to fully contain any signal. Figure 8 shows the RMS of \bar{m} at the different mass points. We scan \bar{m} in steps of $10 \text{ MeV}/c^2$, half the bin size, so that at least one bin will fully contain the signal. Thus, in the \bar{m} range from $0.24 - 5.3 \text{ GeV}/c^2$, there are 507 total bins. We define the signal and background regions in Δm by cutting at a value of Δm so that the signal is 90% efficient, as discussed above.

With this framework, the number of background events in a given \bar{m} bin is quite small. Except at low \bar{m} , the expected number of background events in the entire Δm range is typically below 100 events in a \bar{m} bin, particularly for the $\mu^+\mu^-\mu^+\mu^-$ mode where it is below 5 events. Thus there will be relatively large fluctuations in the background due to Poisson statistics and the limit setting procedure must take this into account. We use a profile likelihood technique[15] to set limits in the presence of nuisance parameters, such as the expected background yield. Using this technique, we obtain a confidence level (CL) for the presence of signal defined as:

$$CL = Prob(-2 \log(\mathcal{L}_{s=0}) - 2 \log(\mathcal{L}_{max})) \quad (4)$$

where $\mathcal{L}_{s=0}$ is the value of the likelihood at 0 signal events and \mathcal{L}_{max} is the maximum value of the likelihood.

Since in our dataset we will have 507 correlated measurements (204 independent measurements), each at a different \bar{m} , we need to determine a criteria for a signal observation. Simply asking whether

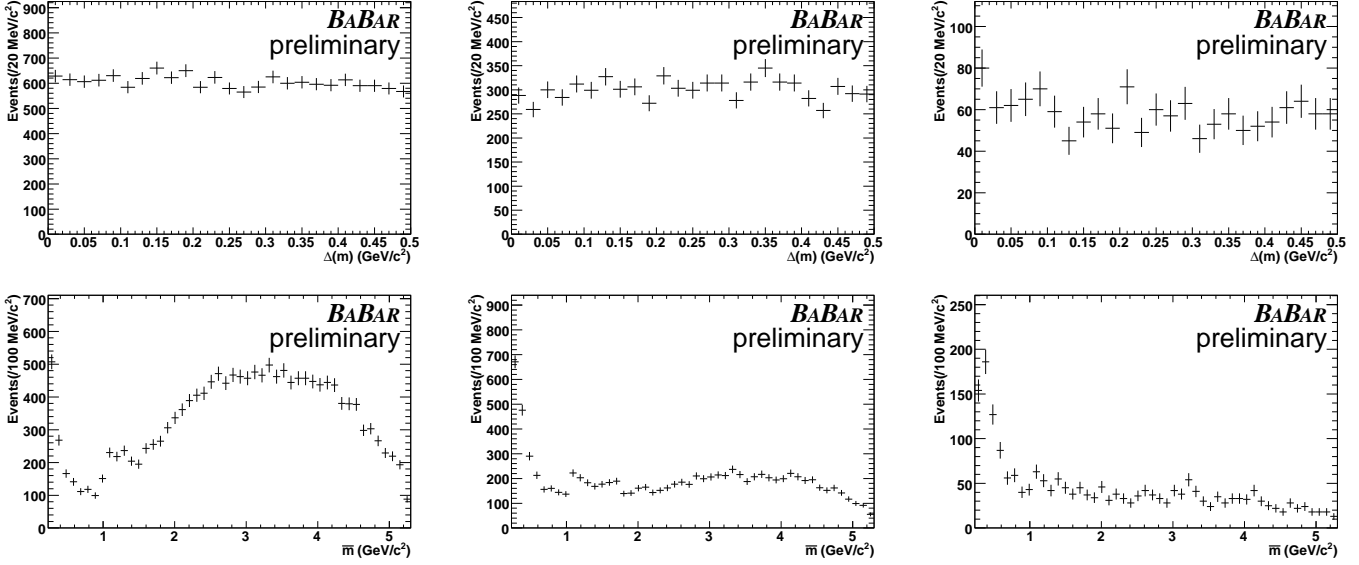


Figure 6: The background (top) Δm and (bottom) \bar{m} distributions for (left-to-right) $e^+e^-e^+e^-$, $e^+e^-\mu^+\mu^-$, and $\mu^+\mu^-\mu^+\mu^-$ from the full dataset. For the Δm plots, we have required $\bar{m} > 1\text{GeV}$ to that all events have the same upper Δm value. The effect of the Δm cut increasing from $0.25\text{ GeV}/c^2$ to $0.5\text{ GeV}/c^2$ at $\bar{m} = 1.0\text{ GeV}/c^2$ can be seen in the \bar{m} plots.

an individual bin has an observed yield in it $> 3\sigma$ above 0 is not enough since the probability to observe at least 1 $> 3\sigma$ fluctuation in one of the \bar{m} bins is 0.3 (as determined from the simulation described below). We need to redefine the $X\sigma$ levels for the new question “What is the chance that I see a background fluctuation above $X\sigma$ in our 507 correlated trials?”. We have done this by generating many simulated datasets (toys) with the expected \bar{m} and Δm background distributions with 0 signal and plotting the highest value of the signal confidence level observed over that dataset, which we call CL_{max} . The results of these simulations are shown in Figure 9, plotting the more convenient variable $-\ln(1 - CL_{max})$. As a reference, the distribution of values $-\ln(1 - CL)$ from a single bin (i.e. not the largest value in an \bar{m} scan) is shown in Figure 10. Table 2 shows the values of $-\ln(1 - CL_{max})$ that correspond to $1-4\sigma$ fluctuations of the background (also displayed

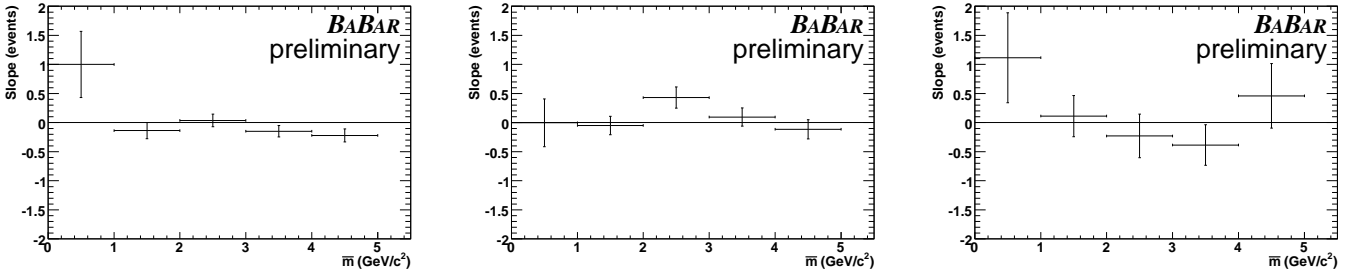


Figure 7: The slope of the background Δm distributions for (left-to-right) $e^+e^-e^+e^-$, $e^+e^-\mu^+\mu^-$, and $\mu^+\mu^-\mu^+\mu^-$ as a function of \bar{m} . The mean values of the slopes are: -0.11 ± 0.06 , 0.07 ± 0.08 , and -0.02 ± 0.19 .

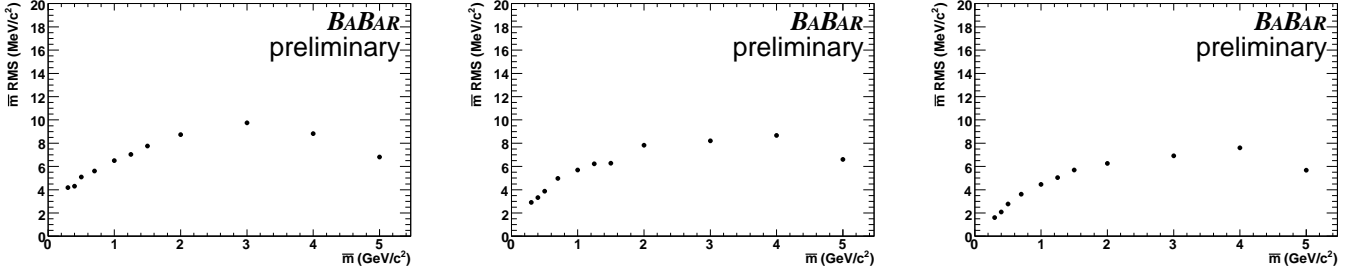


Figure 8: The \overline{m} RMS versus W' mass for (left to right) $W'W' \rightarrow e^+e^-e^+e^-$, $W'W' \rightarrow e^+e^-\mu^+\mu^-$, and $W'W' \rightarrow \mu^+\mu^-\mu^+\mu^-$.

on the plot). Although the background levels are different, the values are consistent between the three modes.

Additionally, we calculate the combined max confidence level, defined as:

$$(1 - CL_{max,C}) = (1 - CL_{max,Ae})(1 - CL_{max,2e2\mu})(1 - CL_{max,4\mu}) \quad (5)$$

whose distribution for background-only toys is shown in the bottom right plot of Figure 9. If lepton universality holds, this limit is potentially more sensitive than the individual confidence levels and allows us to catch a signal that is not significant in any single final state. Our criteria to claim evidence of a signal is to observe the largest value of $-\ln(1 - CL_{max})$ in any of $e^+e^-e^+e^-$, $e^+e^-\mu^+\mu^-$, $\mu^+\mu^-\mu^+\mu^-$ or in the combined confidence level that is greater than the 3σ values given in Table 2.

Table 2: Values of the 1-,2-,3-,4- σ limits for $-\ln(1 - CL_{max})$ in the three final states.

Signif.	$P(CL_{max}) < X$	$-\ln(1 - CL_{max})$			Combined
		$e^+e^-e^+e^-$	$e^+e^-\mu^+\mu^-$	$\mu^+\mu^-\mu^+\mu^-$	
1σ	0.84135	7.2	7.1	7.0	10.2
2σ	0.97725	9.3	9.2	9.0	12.4
3σ	0.99865	12.2	12.1	11.6	15.8
4σ	0.99997	16.3	16.1	14.5	19.2

5 Systematic Errors

There are two types of systematic errors in this analysis: systematics that effect both the yield and cross-section upper limits (e.g. errors due to uncertainties in the background shape) and systematics that just affect the cross-section (e.g. tracking efficiency errors). The second type of error does not effect the signal significance. Table 3 summarizes the values the systematic errors for the different sources described below.

- **Δm background shape:** We assume that the background is uniform in Δm and with our limited MC statistics but we have no *a priori* reason to expect this. While the background Δm does look quite flat and does not appear to depend on \overline{m} , see Figure 7), we still need

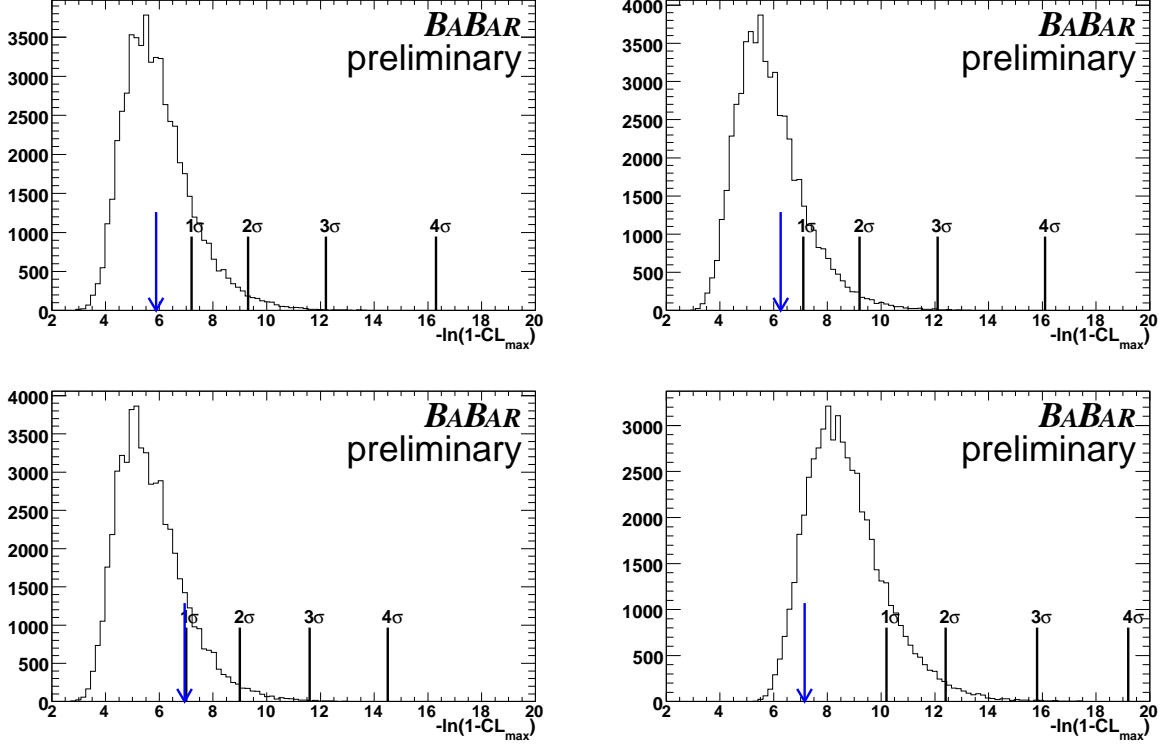


Figure 9: The distribution of $-\ln(1-CL_{max})$ from toy with the arrow showing the value of $-\ln(1-CL_{max})$ observed in data. The plots are (left to right, top to bottom) $e^+e^-e^+e^-$, $e^+e^-\mu^+\mu^-$, $\mu^+\mu^-\mu^+\mu^-$, and the three modes combined.

to account for uncertainties. Consequently, we estimate the Δm background shape from the data itself.

In order to estimate the size of this uncertainty, we have generated toy \overline{m} scans (background only) with a slope and calculated the signal yield assuming a slope of 0. The mean Δm slopes are given in the caption of Figure 7. For this study, we shift the mean value of the slope (B_m) by:

- for $B_m < 0$, we assign the slope to be $B_m - \sigma$
- for $B_m > 0$, we assign the slope to be $-\sigma$

where σ_m is the error on the mean. We only use the negative slope values because we are primarily interested in how this biases us toward more signal. The results of this study are shown in Figure 11 as the observed signal yield bias vs \overline{m} for the three modes. The bias depends on \overline{m} because both the number of background events in the full Δm region and because the Δm signal/background region definitions depend on \overline{m} .

We incorporate this bias into a systematic error on the cross section by converting the bias in the number of events into a cross section in \overline{m} bins. The error is largest for the $e^+e^-e^+e^-$ mode where at high \overline{m} is as large as ~ 5 ab; for the other two modes this error is generally < 1 ab.

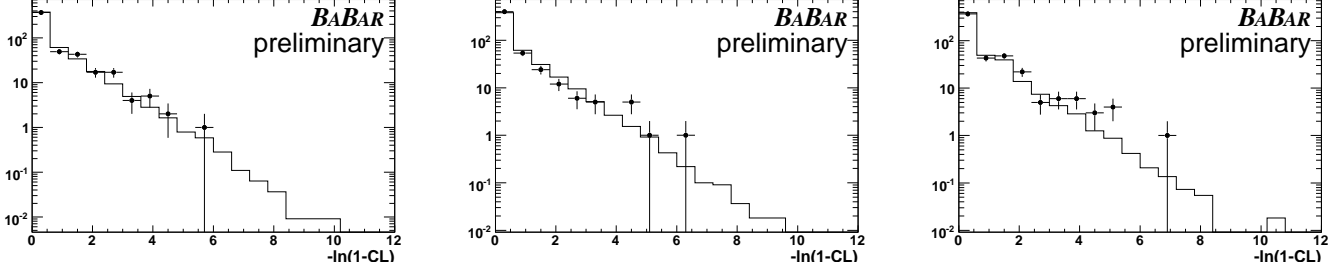


Figure 10: The distribution of values of $-\ln(1 - CL)$ from (error bars) data and (solid histogram) toy for (left to right) $e^+e^-e^+e^-$, $e^+e^-\mu^+\mu^-$, and $\mu^+\mu^-\mu^+\mu^-$.

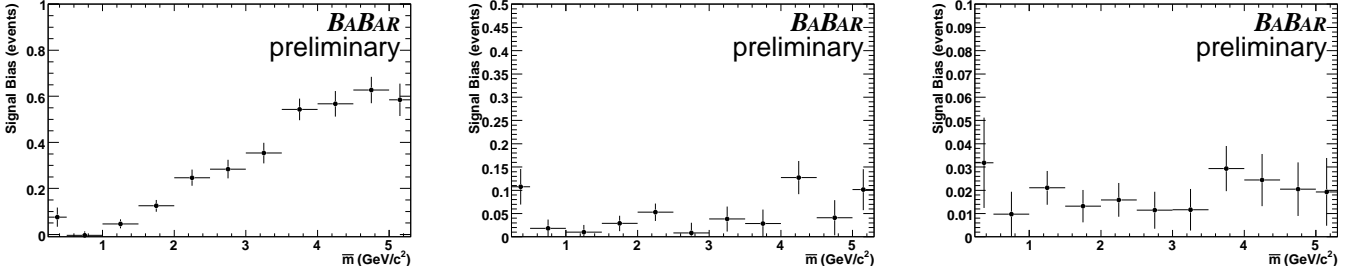


Figure 11: The positive signal yield bias due to the uncertainty in the background Δm slope as a function of \bar{m} for (left-to-right) $e^+e^-e^+e^-$, $e^+e^-\mu^+\mu^-$, and $\mu^+\mu^-\mu^+\mu^-$.

- **Δm signal shape:** We use MC at select mass values to interpolate the 90% efficiency Δm cut value to cover all masses. The interpolation is done with a polynomial and we vary the parameters of the polynomial within their errors to get the error in the Δm cut value. This is then translated into an efficiency error. The magnitude of this error is $\sim 1\%$ and depends slightly on \bar{m} .
- **interpolation of total efficiency:** We use MC at select mass values to interpolate the total efficiency to all masses. The interpolation is done by interpolating the efficiency linearly between the MC mass points. We propagate the errors in the efficiency points due to MC statistics through the interpolation. In addition, we take the difference between a linear and quadratic interpolation and assign the difference, added in quadrature with the statistical error, as the systematic. The magnitude of this error is $\sim 3\%$ and depends slightly on \bar{m} .
- **particle ID:** we assign a 1% error per electron and 2% error per muon on the cross sections to account for the systematic error in the PID efficiency. This is the dominant systematic error.
- **tracking efficiency:** we assign 0.21% error per track on the cross sections to account for the systematic error in the charged track reconstruction efficiency.
- **luminosity:** we assign a 1.1% error on the cross sections due to the uncertainty in the total luminosity.

We add these sources of systematic error in quadrature and scale the statistical 90% upper limit by the fractional systematic error to obtain the final upper limit. This error depends slightly on

\bar{m} but is around 5% for $e^+e^-e^+e^-$ (up to 10% for high \bar{m}), 6.5% for $e^+e^-\mu^+\mu^-$, and 8.2% for $\mu^+\mu^-\mu^+\mu^-$.

Table 3: Sources of systematic uncertainties and their contributions.

Source	$e^+e^-e^+e^-$	$e^+e^-\mu^+\mu^-$	$\mu^+\mu^-\mu^+\mu^-$
Δm bkg shape	0.4-5.5 ab	0.1-0.7 ab	0.1-0.3 ab
Δm signal efficiency	1%	1%	1%
total signal efficiency	3%	3%	3%
particle ID	4%	6%	8%
tracking efficiency	0.8%	0.8%	0.8%
luminosity	1.1%	1.1%	1.1%

6 Results and Conclusions

The spectra for the entire dataset (including the 10% test sample) show no significant signal in any of $e^+e^-e^+e^-$, $e^+e^-\mu^+\mu^-$, $\mu^+\mu^-\mu^+\mu^-$ final states, or the combination of the three. The summary of results is shown in Table 4. The distribution of observed signal events, after background subtraction, for all bins in \bar{m} is shown in Figure 12. The values of $-\ln(1 - CL)$ versus \bar{m} are shown in Figure 13 and show no bins above the 3σ value, shown on the plots. The raw distribution of $-\ln(1 - CL)$ compared to toy simulations with only background is shown in Figure 10 and is in good agreement. The plots in Figure 9 compare the values of the $-\ln(1 - CL_{max})$ observed in data with the distribution found in toy simulation.

Table 4: Summary of the $-\ln(1 - CL_{max})$ observed in data.

	$-\ln(1 - CL_{max})$	\bar{m}_{max} (GeV)
$e^+e^-e^+e^-$	5.88	5.27
$e^+e^-\mu^+\mu^-$	6.26	1.44
$\mu^+\mu^-\mu^+\mu^-$	6.94	2.23
Combined	7.15	1.66

Correcting for efficiency (Figure 3, using linear interpolation between points and including the 90% cut on Δm) and scaling by the luminosity, we obtain a 90% upper limit for the cross section as shown in Figures 14 and 15. The points in these plots are the upper limit for each bin in \bar{m} while the solid lines are the averages of the upper limits in the \bar{m} region shown. We set upper limits of $\sigma(e^+e^- \rightarrow W'W' \rightarrow e^+e^-e^+e^-) < (15 - 70)$ ab, $\sigma(e^+e^- \rightarrow W'W' \rightarrow e^+e^-\mu^+\mu^-) < (15 - 40)$ ab, and $\sigma(e^+e^- \rightarrow W'W' \rightarrow \mu^+\mu^-\mu^+\mu^-) < (11 - 17)$ ab depending on W' mass (taking the ranges from the averaged limits).

Assuming lepton universality ($BR(W' \rightarrow e^+e^-) = BR(W' \rightarrow \mu^+\mu^-)$), we combine the three modes to obtain upper limits for the reaction $e^+e^- \rightarrow W'W' \rightarrow l^+l^-l'^+l'^-$. We obtain this limit by combining the individual profile likelihood functions for the three decay modes as a function of

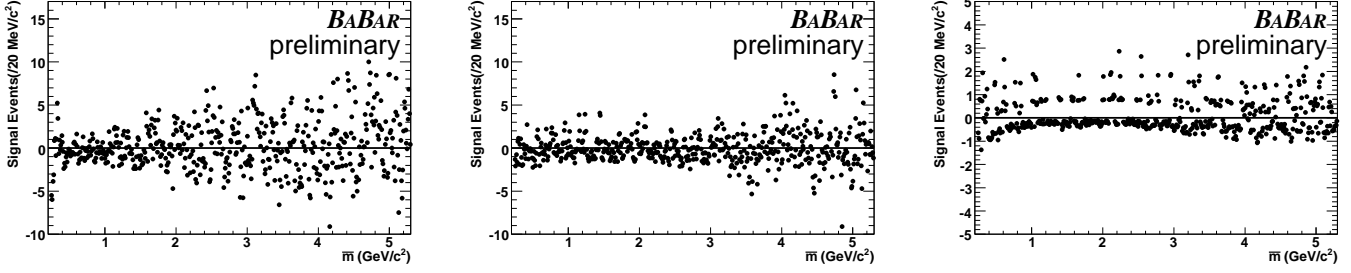


Figure 12: The number of signal events after background subtraction versus \bar{m} for (left to right) $e^+e^-e^+e^-$, $e^+e^-\mu^+\mu^-$, and $\mu^+\mu^-\mu^+\mu^-$. The band structure evident in the $\mu^+\mu^-\mu^+\mu^-$ plot is due to the very low number of events in this mode.

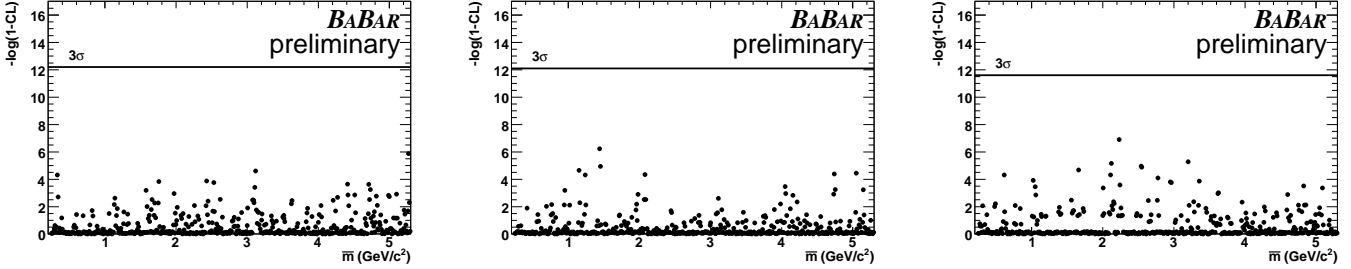


Figure 13: The value of $-\ln(1 - CL)$ versus \bar{m} for (left to right) $e^+e^-e^+e^-$, $e^+e^-\mu^+\mu^-$, and $\mu^+\mu^-\mu^+\mu^-$.

$e^+e^- \rightarrow W'W' \rightarrow l^+l^-l'^+l'^-$ cross section. The combined upper limit is shown in Figure 15; we set upper limits for $\sigma(e^+e^- \rightarrow W'W' \rightarrow l^+l^-l'^+l'^-) < (25 - 60)$ ab.

From the combined upper limit, we derive limits on the possible couplings between the Standard Model and dark sectors. The cross section for $e^+e^- \rightarrow W'W'$ has been calculated by Essig *et al.*[10]. For a dark photon A' mass less than the center of mass energy, E_{cm} , the cross section is given by:

$$\sigma(e^+e^- \rightarrow W'W')_{low} = N_c \frac{4\pi}{3} \frac{\varepsilon^2 \alpha_D \alpha}{E_{cm}^2} \sqrt{1 - \frac{4m_{W'}^2}{E_{cm}^2}} \left(1 + \frac{2m_{W'}^2}{E_{cm}^2} \right) \quad (6)$$

while for an A' mass larger than E_{cm} the cross section is:

$$\sigma(e^+e^- \rightarrow W'W')_{high} = N_c \frac{4\pi}{3} \frac{\varepsilon^2 \alpha_D \alpha}{E_{cm}^2} \frac{E_{cm}^4}{m_{A'}^4} \sqrt{1 - \frac{4m_{W'}^2}{E_{cm}^2}} \left(1 + \frac{2m_{W'}^2}{E_{cm}^2} \right) \quad (7)$$

where N_c is the number of colors in the dark sector, ε is the mixing parameter between the SM and the dark sector, and α_D is the dark sector coupling constant. Figure 16 shows the upper limits we obtain on $\varepsilon^2 \alpha_D$ assuming low A' mass, or on $\frac{\varepsilon^2 \alpha_D}{m_{A'}^4}$ assuming large A' mass. For most of the mass range, we exclude values of $\varepsilon^2 \alpha_D$ above 2×10^{-10} in the low A' mass scenario or values of $\frac{\varepsilon^2 \alpha_D}{m_{A'}^4}$ above 2×10^{-14} in the high A' mass scenario. In the model of Ref [10], these limits exclude the preferred parameter region for A' masses above $1.0 \text{ GeV}/c^2$.

We would like to thank Rouven Essig, Philip Schuster, and Natalia Toro for useful discussions and for generating the signal Monte Carlo samples. We are grateful for the extraordinary con-

tributions of our PEP-II colleagues in achieving the excellent luminosity and machine conditions that have made this work possible. The success of this project also relies critically on the expertise and dedication of the computing organizations that support *BABAR*. The collaborating institutions wish to thank SLAC for its support and the kind hospitality extended to them. This work is supported by the US Department of Energy and National Science Foundation, the Natural Sciences and Engineering Research Council (Canada), the Commissariat à l’Energie Atomique and Institut National de Physique Nucléaire et de Physique des Particules (France), the Bundesministerium für Bildung und Forschung and Deutsche Forschungsgemeinschaft (Germany), the Istituto Nazionale di Fisica Nucleare (Italy), the Foundation for Fundamental Research on Matter (The Netherlands), the Research Council of Norway, the Ministry of Education and Science of the Russian Federation, Ministerio de Educación y Ciencia (Spain), and the Science and Technology Facilities Council (United Kingdom). Individuals have received support from the Marie-Curie IEF program (European Union) and the A. P. Sloan Foundation.

References

- [1] J. Chang *et al.*, Nature **456**, 362 (2008).
- [2] A. A. Abdo *et al.* [The Fermi LAT Collaboration], arXiv:0905.0025 [astro-ph.HE].
- [3] O. Adriani *et al.* [PAMELA Collaboration], Nature **458**, 607 (2009).
- [4] I. V. Moskalenko and A. W. Strong, AIP Conf. Proc. **801**, 57 (2005).
- [5] D. Hooper, P. Blasi and P. D. Serpico, JCAP **0901**, 025 (2009).
- [6] N. Arkani-Hamed, D. P. Finkbeiner, T. R. Slatyer and N. Weiner, Phys. Rev. D **79**, 015014 (2009).
- [7] P. Jean *et al.*, Astron. Astrophys. **407**, L55 (2003).
- [8] R. Bernabei *et al.*, Eur. Phys. J **C56**,333 (2008).
- [9] B. Batell, M. Pospelov, A. Ritz arXiv:0903.0363 [hep-ph].
- [10] R. Essig, P. Schuster and N. Toro, arXiv:0903.3941 [hep-ph].
- [11] J. Alwall *et al.*, JHEP **0709**, 028 (2007).
- [12] F.A. Berends *et al.*, Nucl. Phys. B253 (1985) 441.
- [13] *BABAR* Collaboration, B. Aubert *et al.*, Nucl. Instrum. Methods Phys. Res., Sect. A **479**, 1 (2002).
- [14] GEANT4 Collaboration, S. Agostinelli *et al.*, Nucl. Instrum. Methods Phys. Res., Sect. A **506**, 250 (2003).
- [15] W.Rolke, A. Lopez, J. Conrad and F. James, Nucl. Instrum. Methods Phys. Res., Sect. A **551**, 493 (2005).

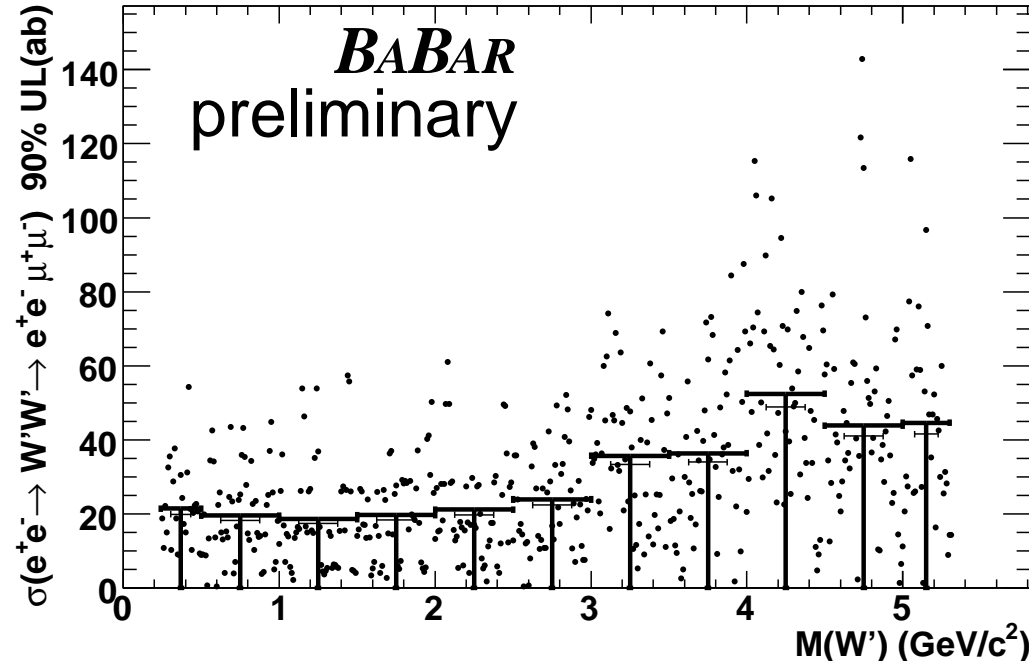
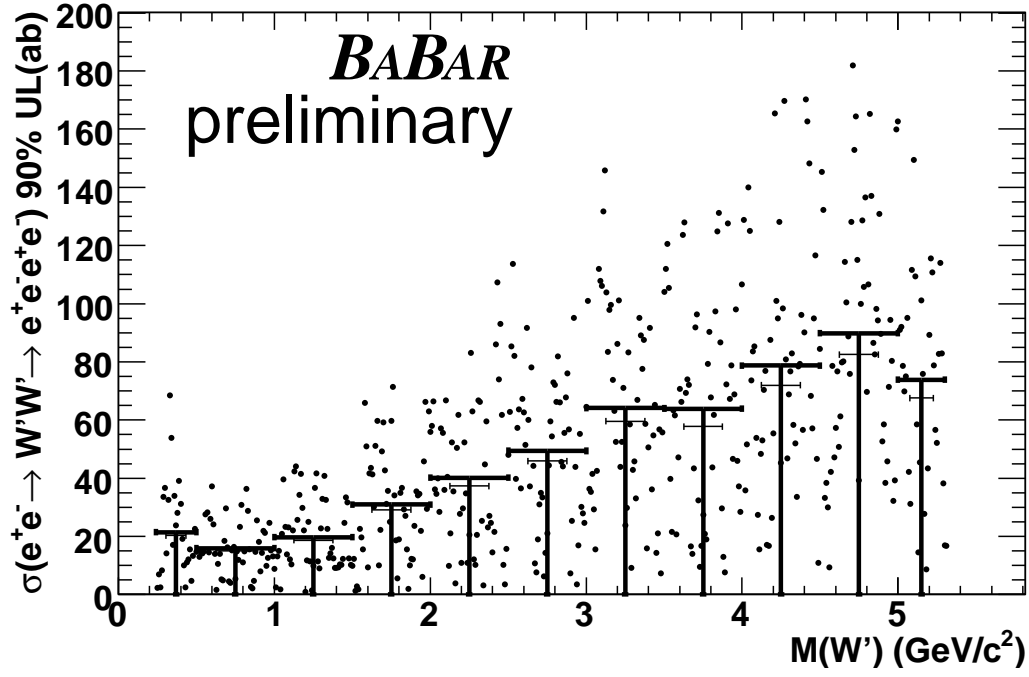


Figure 14: The cross section 90% upper limit versus \bar{m} for (top to bottom) $e^+e^- \rightarrow W'W' \rightarrow e^+e^-e^+e^-$ and $e^+e^- \rightarrow W'W' \rightarrow e^+e^- \mu^+ \mu^-$. The points are the upper limit for each \bar{m} bin while the lines are the average of the limits over many bins.

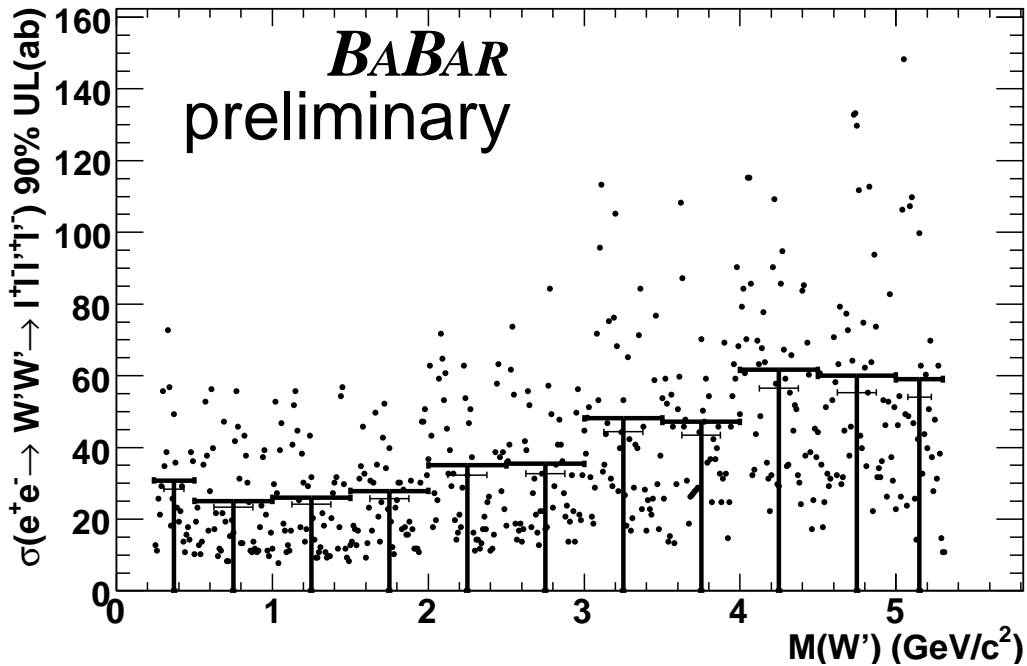
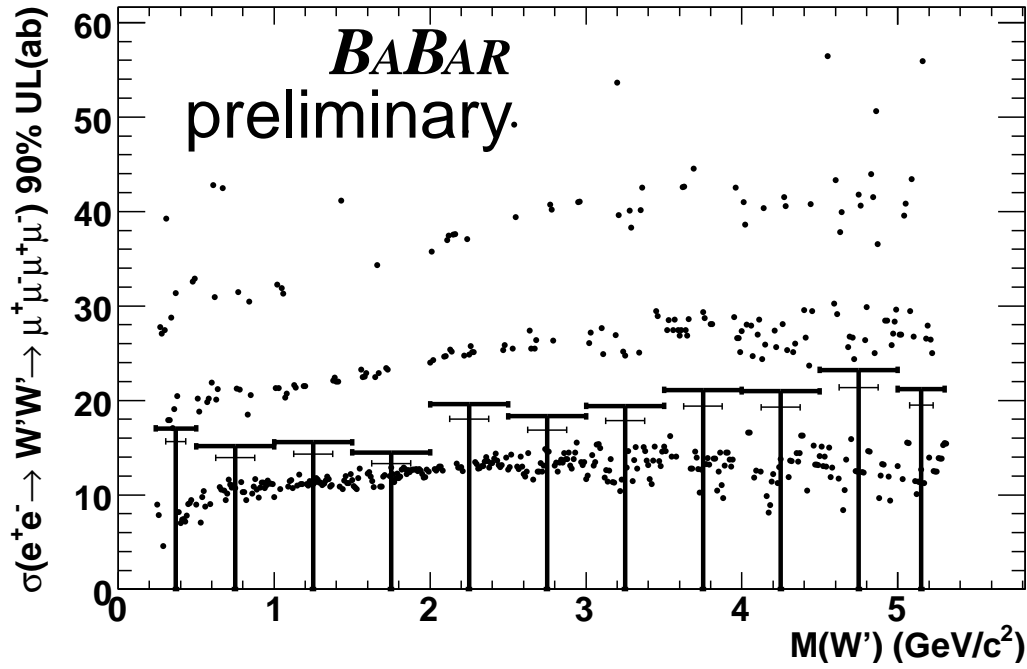


Figure 15: The cross section 90% upper limit versus \bar{m} for (top to bottom) $e^+e^- \rightarrow W'W' \rightarrow \mu^+\mu^-\mu^+\mu^-$ and the combined $e^+e^- \rightarrow W'W' \rightarrow l^+l^-l^+l^-$ assuming lepton universality. The points are the upper limit for each \bar{m} bin while the lines are the average of the limits over many bins. The band structure evident in the $\mu^+\mu^-\mu^+\mu^-$ plot is due to the very low number of events in this mode.

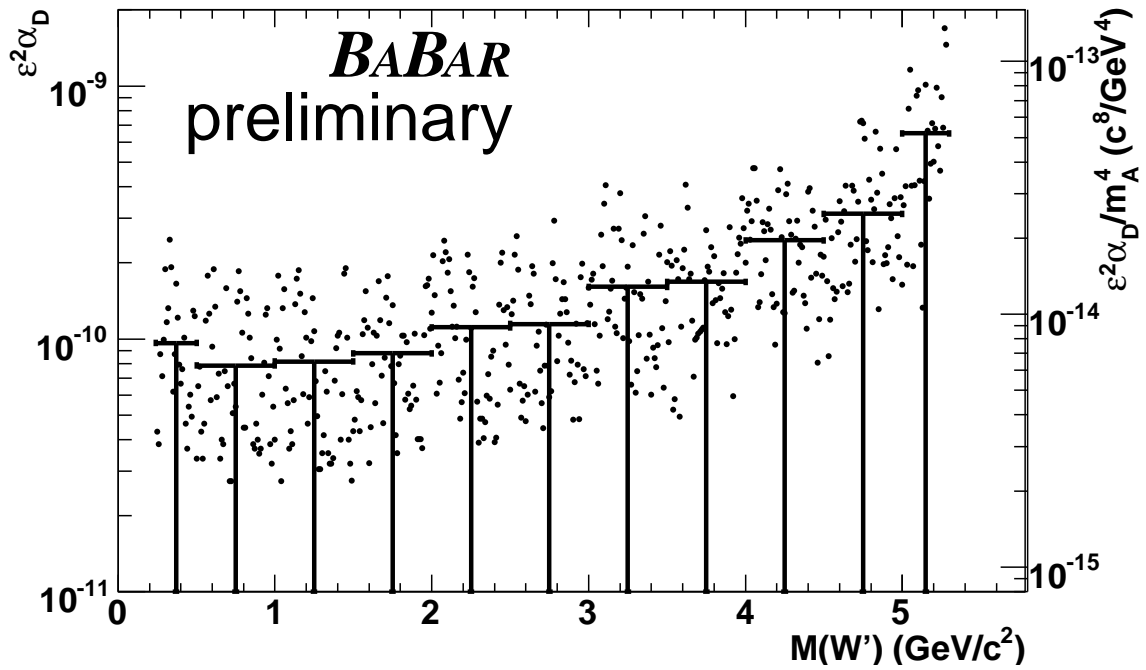


Figure 16: The 90% upper limit on $\epsilon^2\alpha_D$ (left axis) or $\frac{\epsilon^2\alpha_D}{m_{A'}^4}$ (right axis) versus $m(W')$. The points are the upper limit for each $m(W')$ bin while the lines are the average of the limits over many bins.